CMS Technical Summary Report #90-14

NEW TRANSIENT ALGORITHMS FOR NON-NEWTONIAN FLOWS

David S. Malkus,
Yi-Cheng Tsai,
and
Robert W. Kolkka

UNIVERSITY OF WISCONSIN

CENTER FOR THE MATHEMATICAL SCIENCES

Center for the Mathematical Sciences
University of Wisconsin—Madison
610 Walnut Street
Madison, Wisconsin 53705

October 1989

(Received October 11, 1989)

Sponsored by

U. S. Army Research Office
P. O. Box 12211
Research Triangle Park
North Carolina 27709

Air Force Office of
Scientific Research
Washington, DC 20332

National Science Foundation
Washington, DC 20550

UNIVERSITY OF WISCONSIN-MADISON
CENTER FOR THE MATHEMATICAL SCIENCES

NEW TRANSIENT ALGORITHMS FOR NON-NEWTONIAN FLOWS *

David S. Malkus[1]
Yi-Cheng Tsai[1]
Robert W. Kolkka [2]

CMS Technical Summary Report #90-14
October 1989

Abstract

A fully dynamic method for shear flows is presented that treats the short time-scales associated with Newtonian viscosity (or short relaxation processes) and shear-wave propagation implicitly, while treating the long relaxation processes explicitly. The method is generalized to flows with non-constant strain-rate histories in the context of the well-known fiber-drawing problem. The linearized stability of the methods is analyzed, and extension of these methods to planar flows is given. The approach taken in the case of non-trivial deformation histories is that of an Oldroyd difference quotient (ODQ) that approximates the convected derivatives of the differential constitutive equation in Lagrangian fashion along the portion of the streamline upstream of the stress evaluation point. Techniques based on earlier ideas of drift-function tracking are used to develop a weighting scheme for the ODQ that permits the use of low order, C_0 stress elements. The numerical methods are discussed and analyzed in the context of a Johnson-Segalman fluid model with added Newtonian viscosity. The resulting initial-boundary-value problem is globally well-posed and possesses the key feature: the steady shear stress is a non-monotone function of the strain rate. Such models will be seen to display the spurt phenomenon in plane Poiseuille flow and apparently related phenomena in step strain experiments. Analysis of the numerical methods shows that the ratio of short to long relaxation times or the Newtonian viscosity ratio is a key parameter in the stability and accuracy of the methods. When this is properly accounted for the techniques described here work well in shear and extensional flows and show promise for two-dimensional flows.

AMS (MOS) Subject Classifications: 35L60, 65M05, 65M10, 65M60, 73F15, 76A05, 76A10

Key Words: explicit, fiber drawing, finite element, finite difference, implicit, instability, linearized stability, Newtonian viscosity, non-monotone shear stress, Oldroyd Difference Quotient, relaxation process, shear flow, spurt, step strain

* Supported by the U. S. Army Research Office under Grant DAAL03-87-K-0036, the Air Force Office of Scientific Research under Grants AFOSR-85-0141, AFOSR-87-0191, and AFOSR-89-0220 and the National Science Foundation under Grants DMS-8620303, DMS-8712058, DMS-8907264 and CTS-8910518.

[1] Also Department of Engineering Mechanics.

[2] Fluids Research Oriented Group, Department of Mathematics, and Department of Chemical Engineering Michigan Technological University Houghton, MI49931-1295.

A-1

1. INTRODUCTION

We consider the equations of motion, stress, and continuity for a Johnson-Segalman fluid [1] with added Newtonian viscosity. The Johnson-Segalman model should be viewed as a simple constitutive equation representing features which are characteristic of non-monotone stress/strain-rate constitutive relations [2 – 10] (see Fig. 1); many other models have these features, and some are known to produce the kind of dramatic and interesting rheological behavior discussed in this paper in the context of Johnson-Segalman [2,4,6]. There is some controversy among rheologists as to whether the predictions of such models are physically correct; we believe so, and have argued our case extensively elsewhere [2,4 – 7,10]. Our thrust here is numerical, and we aim to develop methods of general applicability to models with and without non-monotone behavior. At very least, the success of our methods in shearing flows in the 'spurt' regime induced by non-monotonicity can be viewed as pushing the numerical method to the limit in order to test its robustness in the presence of strong instabilities.

The equations of motion, stress, and continuity in terms of velocity, $\mathbf{v}$, total stress, $\mathbf{S}$, extra stress, τ, strain rate, $\dot{\mathbf{e}}$, and pressure, p, for the Johnson-Segalman model are

$$\begin{cases} \alpha \left[\frac{\partial \mathbf{v}}{\partial t} + (\mathbf{v}\cdot\nabla)\,\mathbf{v}\right] = \nabla\cdot\mathbf{S} \\ \mathbf{S} = -p\,I + 2\varepsilon\dot{\mathbf{e}} + \tau \\ \frac{\mathcal{D}_a\tau}{\mathcal{D}t} + \tau = 2\dot{\mathbf{e}} \\ \frac{\mathcal{D}_a\tau}{\mathcal{D}t} := \frac{\partial\tau}{\partial t} + (\mathbf{v}\cdot\nabla)\,\tau - \tau\nabla\mathbf{v} - (\nabla\mathbf{v})^T\tau + (1-a)(\tau\dot{\mathbf{e}} + \dot{\mathbf{e}}\tau) \\ \nabla\cdot\mathbf{v} = 0\ . \end{cases} \tag{1}$$

The equations are in nondimensional form; α is a ratio of Reynolds number to Deborah number; time has been scaled by the dominant relaxation time; ε is the ratio of Newtonian viscosity to polymer zero shear viscosity or, alternatively, the ratio of dominant to secondary relaxation time; the dimensional form of the equations and further details of the dimensional analysis may be found in Refs. [2] and [5]. The parameter, a, is a nondimensional number that relates the motion of the polymer molecules to the mean motion of the continuum; this motion is non-affine when $a \neq 1$; we consider only $a > 0$ here. In Refs. [5,6,7], it is shown that the Newtonian viscosity term is generally representative of the presence of shorter relaxation times, widely separated from the dominant relaxation time that can occur in pure polymer systems as well as polymer/solvent systems.

In Refs. [5,6,7], the reduction of Eqs. (1) to transient shear flows is discussed. Following Ref. [5], for $a < 1$ one may also scale σ, v, and f by $(1-a^2)^{1/2}$; the result is

$$\begin{cases} \alpha v_t = \sigma_x + \varepsilon v_{xx} + f \\ \sigma_t = (Z+1)\,v_x - \sigma \\ Z_t = -\sigma v_x - Z\ . \end{cases} \tag{2}$$

In the absence of Newtonian viscosity (i.e., when $\varepsilon = 0$), the system (2) is hyperbolic as long as $Z + 1 \geq 0$, and the speeds, c, are

$$c = 0,\ \pm\sqrt{\frac{Z+1}{\alpha}}\ . \tag{3}$$

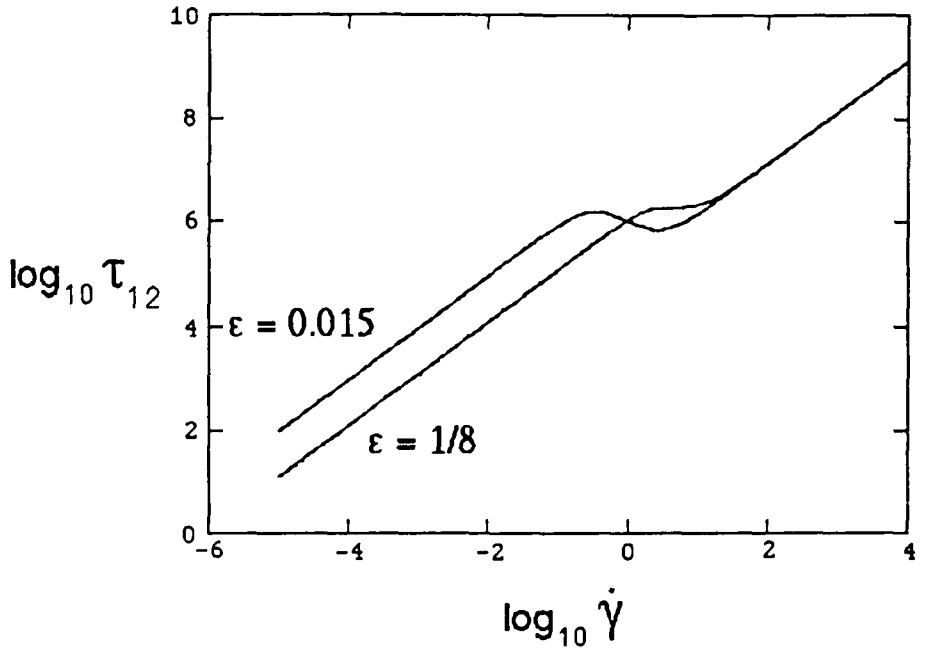

Fig. 1 Stress vs. strain-rate for a Johnson-Segalman model. Dimensional units; values characteristic of actual materials. Values of ε give neutrally stable (1/8) and critical cases (0.015); $\dot{\gamma} = 2\dot{e}_{12}$.

Otherwise the system has elliptic character, and the type change corresponds to a loss of evolutionarity. When Newtonian viscosity is present (i.e., when $\varepsilon \neq 0$), it can be shown that the system is always evolutionary [8,9]. When Newtonian viscosity is absent the system can exhibit Hadamard instabilities [8,9].

2. NEW TRANSIENT ALGORITHMS FOR SHEAR FLOW

In this section we briefly describe two test problems that are solved by our numerical techniques for shear flow. We then describe the numerical method, arrange the algorithm in suitable form for a linearized 'matrix' stability analysis [11,12], and derive the resulting stability bounds.

A. Spurt: In Refs. [2,4 – 7], the phenomenon of spurt observed by Vinogradov, et al. [13] is modeled exploiting the non-monotonicity of the Johnson-Segalman models steady stress vs. strain-rate curve, using system (2) and boundary conditions appropriate for pressure-driven flow (see Fig. 2). The phenomenon of the dramatic increase in capillary or die throughput at a fixed critical stress, independent of molecular weight, can be reproduced with remarkable accuracy. The resulting flow regime is characterized by a layer of high shear rate near the wall, in which the extra stress plays virtually no role in equilibrating the driving pressure gradient. Outside the layer, the longer relaxation process is the dominant load-bearing mechanism. During the process of spurt, there are large oscillations in stress and shear rate, and material points that end up inside the layer are alternately subjected to high and low rates of shear until effective steadiness is achieved.

B. Step strains: We consider an idealized model of the classical step strain experiment

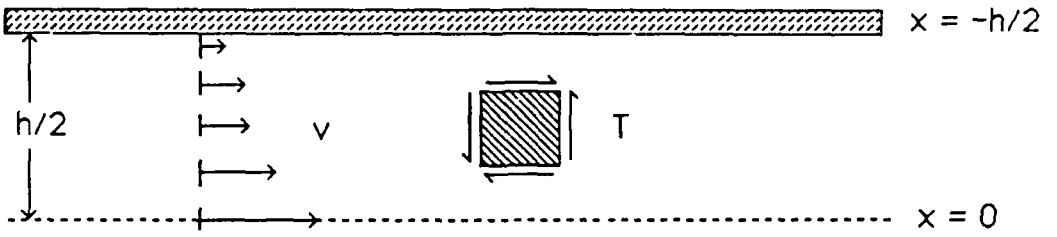

Fig. 2. Problem domain for channel flow driven by a pressure gradient (plane Poiseuille flow). The dimension, $h/2$, is scaled to 1/2 in the nondimensional equations. $T = \sigma + \varepsilon v_x$ is the total shear stress.

[3,10,14,15] that combines Eqs. (2) with boundary conditions

$$\begin{cases} v(0,t) = 0 \\ v(1,t) = \dot{g}(t) \\ \sigma_x(0,t) + \varepsilon v_{xx}(0,t) = 0 \, . \end{cases} \tag{4}$$

We thus have Couette flow [3] in which the upper wall is a plate that moves suddenly, shortly after time $t = 0$. The picture is similar to Fig. 2, with the symmetry line replaced by the fixed wall, whose coordinate is taken to be $x = 0$ in nondimensional units; the moving wall is at $x = 1$ (see Fig. 5, below). The classical problem is properly posed [10] by taking the limit of the sequence of solutions to this problem as g tends to a multiple of the Heaviside function, which is the step in strain, γ, based on plate motion. In this context, we can see the consequences of adding an arbitrarily small amount of Newtonian viscosity, ε, or omitting this term. We consider the Lodge-Meissner function:

$$\Phi(\gamma) = \lim_{t \to \infty} \frac{\tau_{11} - \tau_{22}}{\gamma \, S_{12}} = -\frac{2Z}{\hat{\gamma} T} \, . \tag{5}$$

where $T := \sigma + \varepsilon v_x$, and $\hat{\gamma}$ is the strain calculated from system (3), which is a factor of $(1 - a^2)^{1/2}$ smaller than the corresponding strain of system (1) (the $a = 1$ case is treated as a special case). Note that the total shear stress, S_{12} or T, appears in the denominator of Eq. (5). Eq. (5) was intended to apply in situations where there is no flow with relaxing stresses and thus where there is no difference between S_{12} and τ_{12} (or T and σ): here we have chosen to use the physically measurable, total stress, for reasons that will become clear later. The Lodge-Meissner relation [10,14,15] states that the limit of Φ as the step becomes instantaneous is observed to be 1 in real polymer systems. For the Johnson-Segalman model, Eq. (5) can be evaluated analytically, under the assumption that momentum effects can be ignored (even though the step is assumed to be instantaneous) and the flow remains homogeneous for all time [10]. The result is plotted in Fig. 3. The Johnson-Segalman model has been criticized for the obvious failure to satisfy the Lodge-Meissner relation and the fact that the shear stress evidently changes sign as a function of strain, as evidenced by the pole in Fig. 3.

C. The numerical method for shear flow: In these shear-flow examples, Newtonian viscosity dominates in high shear-rate regions or times; there the Eqs. (2) have the parabolic

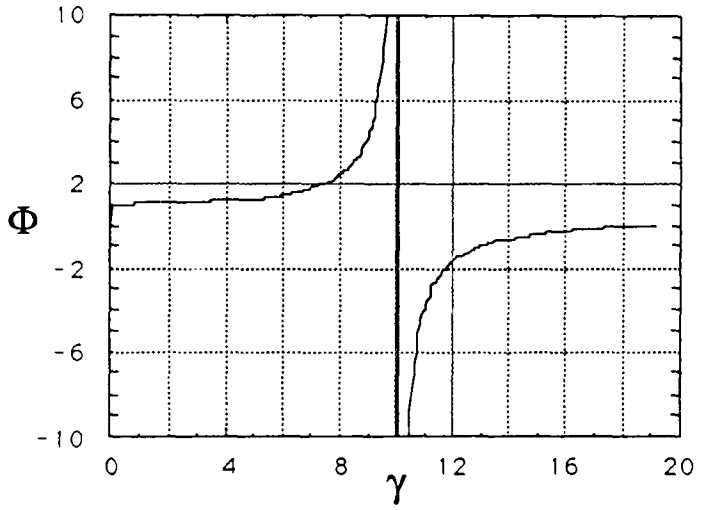

Fig. 3. The Lodge-Meissner function with $a = 0.95$. Values for $\gamma < 5$ are close to 1. The pole is at $\gamma \approx 10$. Another pole is at $\gamma \approx 30$; poles periodically repeat.

character of Newtonian flow; implicit treatment of Newtonian viscosity is essential. In the regions or times of lower shear-rate, where the longer relaxation time dominates, there is wave propagation at the elastic wave speed given by Eq. (3), and the equations, though not formally classifiable, behave like a hyperbolic system with a small amount of added viscous damping. For high polymers of the type used by Vinogradov, et al. [13], the wave speed is finite but very high, and numerical methods must respect it by either the time-step restrictions of explicit integration or the cost of implicit integration. On the other hand, phenomena such as the latent development of spatial inhomogeneity in step strains take place in several step rise-times; phenomena like Vinogradov's spurt take time on the order of many dominant relaxation times to unfold. In either case, the time scale of the interesting physical phenomenon is orders of magnitude longer than wave traversal times. To capture such phenomena by explicit methods, controlled by element wave traversal times, is totally out of the question. The following method was developed to confront this difficulty without requiring implicit iteration on the nonlinearities [2,5].

— *Spatial discretization:* We use standard finite element interpolations [11,12]. In what follows, the definitions of shape functions, matrices, etc. are at the global (rather than element) level. The shape functions are linear, one basis function per node, as picture in Fig. 4. Following standard practice, the nodal values, v_i, are functions of time alone, and the shape functions, N_i, are functions of space alone:

$$[N_1(x), N_2(x), \ldots, N_M(x)] = [N]$$
$$v \cong [N] \begin{Bmatrix} v_1(t) \\ v_2(t) \\ \vdots \\ v_M(t) \end{Bmatrix} = [N]\{v\} \ . \tag{6}$$

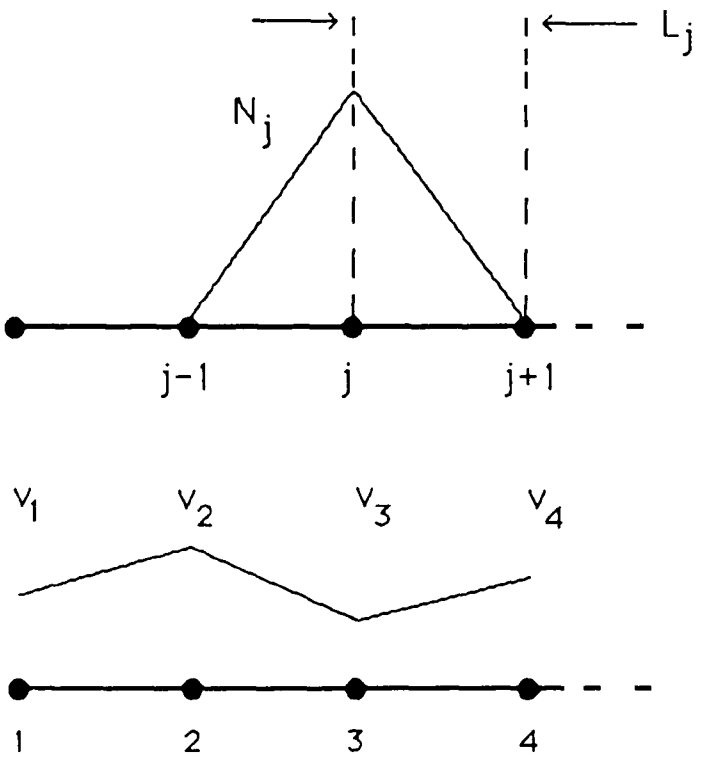

Fig. 4. Velocity trial/test functions for Galerkin method. The N_j are basis functions for piecewise linear approximations for velocity. Stresses are assumed to be piecewise constant on cells between nodes; cells have length L_j and may vary in size.

We use standard "B-Matrix" notation for the matrix relating strain rates to nodal values. Thus

$$v_x \cong [B]\{v\} = [N_{1,x}, N_{2,x}, \ldots, N_{M,x}]\{v\} \ . \tag{7}$$

The acceleration can be written as follows:

$$v_t \cong [N] \begin{Bmatrix} v_{1,t} \\ v_{2,t} \\ \vdots \\ v_{M,t} \end{Bmatrix} = [N]\{\dot{v}\} \ . \tag{8}$$

The viscoelastic contribution to momentum diffusion is

$$\int_0^l \phi_x \sigma dx = \int_o^l \{\phi\}^T [B]^T \sigma dx \ , \tag{9}$$

in which we shall assume σ is elementwise constant. The Galerkin form of the momentum equation is

$$\int_0^l \alpha\phi v_t dx + \int_o^l \phi_x \sigma dx + \varepsilon \int_0^l \phi_x v_x dx = 0 \ , \tag{10}$$

for all admissible ϕ, at each $t > 0$. When the admissible test functions, ϕ, are expanded in terms of the N_i, the spatial discretization of momentum equation becomes [11,12]

$$[M]\{a\} + \varepsilon[K]\{v\} + \{W\} = \{\mathbf{0}\} \ , \tag{11}$$

where

$$\begin{aligned}
\{a\} &= \frac{\partial}{\partial t}\{v\} = \{\dot{v}\} \\
[M] &= \int_0^l \alpha[N]^T[N]\, dx \\
\{W\} &= \int_0^l [B]^T \sigma \, dx \\
[K] &= \int_0^l [B]^T[B]\, dx \\
[N] &= [N_1(x), N_2(x), \ldots, N_M(x)] \\
[B] &= [N_{1,x}, N_{2,x}, \ldots, N_{M,x}] \ .
\end{aligned} \tag{12}$$

— *Time differencing:* The time differencing is based on a standard generalized trapezoidal scheme [11,12].

$$\{v_{n+1}\} \cong \{v_n\} + \Delta t\,[(1-\zeta)\{a_n\} + \zeta\{a_{n+1}\}] \ , \tag{13}$$

where $\zeta > 0$ is a parameter of the method. A predictor for the viscoelastic contribution to the shear stress (the extra stress) is given by a mixed difference, forward on the stress and nonlinear terms and backward on the linear strain-rate term. Z and σ are assumed to be constant on each element and advanced by

$$\frac{\sigma_{n+1} - \tilde{\sigma}_n}{\Delta t} = Z_n (v_x)_n + (v_x)_{n+1} - \tilde{\sigma}_n \ . \tag{14}$$

The momentum equation is solved based on this prediction, and a corrector/Z-update cycle is used for both stress equations.

$$\frac{\tilde{\sigma}_{n+1} - \tilde{\sigma}_n}{\Delta t} = (Z_n + 1)(v_x)_{n+1} - \tilde{\sigma}_n \tag{15}$$

$$\frac{Z_{n+1} - Z_n}{\Delta t} = -\tilde{\sigma}_{n+1}(v_x)_{n+1} - Z_n \ . \tag{16}$$

Combining the space and time discretization of the momentum equation, we have

$$[M]\{a_{n+1}\} + \varepsilon[K]\{v_{n+1}\} + \{W_{n+1}\} = \{\mathbf{0}\} \ , \tag{17}$$

where $\{W_{n+1}\}$ is a predictor of the viscoelastic contribution,

$$\{W_{n+1}\} = \int_0^l [B]^T \sigma_{n+1}\, dx \ . \tag{18}$$

With the discretization of system (2), whose stability is analyzed below, corrector is not used, and there are no "$\sim$"ed corrected quantities. We thus have

$$\frac{\sigma_{n+1} - \sigma_n}{\Delta t} = Z_n (v_x)_n + (v_x)_{n+1} - \sigma_n \ , \tag{19}$$

and Z given by Eq. (16) (with $\tilde{\sigma}_{n+1}$ replaced by σ_{n+1}). It is possible to apply the σ-corrector in the frozen Z case, but numerical experiments show that this procedure is less stable than the one analyzed here. Furthermore, experiments also show the nonlinear algorithm with the predictor-corrector scheme "nearly" unconditionally stable when parameters are selected according to frozen Z analysis, without the corrector step. We should emphasize that we are analyzing a somewhat simpler algorithm – without the correction cycle – to approximate the behavior of the more complicated algorithm. Experience shows that this is a valid simplification.

— *Computational arrangement(momentum):* When we use Eq. (19) to predict σ_{n+1} in Eq. (17), the result is

$$\begin{aligned} \{W_{n+1}\} &= \int_0^l [B]^T \sigma_{n+1}\, dx \\ &= \Delta t [K]\{v_{n+1}\} + \Delta t \int_0^l Z_n [B]^T [B]\{v_n\}\, dx + (1 - \Delta t) \int_0^l [B]^T \sigma_n\, dx \ . \end{aligned} \tag{20}$$

Substitution into momentum equation yields

$$[M]\{a_{n+1}\} + (\varepsilon + \Delta t)[K]\{v_{n+1}\} + \{\tilde{W}_{n+1}\} = \{\mathbf{0}\} \ , \tag{21}$$

where

$$\{\tilde{W}_{n+1}\} := \Delta t \int_0^l \overbrace{Z_n [B]^T [B]\{v_n\}}^{Z-\text{term}}\, dx + (1 - \Delta t) \int_0^l [B]^T \sigma_n\, dx \ . \tag{22}$$

Note that the for frozen coefficient system (2), the Z-term in $\{\tilde{W}_{n+1}\}$ can be written as $\Delta t Z [K]\{v_n\}$.

— *A recursion for* $\{\tilde{W}_{n+1}\}$: From Eq. (20) and the definition of $\{\tilde{W}_{n+1}\}$, we have

$$\int_0^l [B]^T \sigma_{n+1}\, dx = \Delta t [K]\{v_{n+1}\} + \{\tilde{W}_{n+1}\} \ . \tag{23}$$

Cycling back to n+1 $\rightarrow$ n yields

$$\int_0^l [B]^T \sigma_n\, dx = \Delta t [K]\{v_n\} + \{\tilde{W}_n\} \ . \tag{24}$$

We substitute into definition of $\{\tilde{W}_{n+1}\}$ to get

$$\{\tilde{W}_{n+1}\} = (1-\Delta t)\{\tilde{W}_n\} + \Delta t(1-\Delta t)[K]\{v_n\} + \Delta t \int_0^l Z_n[B]^T[B]\{v_n\}\,dx \ . \tag{25}$$

In the frozen Z case, Eq. (25) becomes

$$\{\tilde{W}_{n+1}\} = (1-\Delta t)\{\tilde{W}_n\} + (Z + (1-\Delta t))\Delta t[K]\{v_n\} \ . \tag{26}$$

— *Quasilinear difference equations:* The fully nonlinear system (1) can now be written in recursive form,

$$\begin{gathered}
[M]\{a_{n+1}\} + (\varepsilon + \Delta t)[K]\{v_{n+1}\} + \{\tilde{W}_{n+1}\} = \{\mathbf{0}\} \\
\{\tilde{W}_{n+1}\} = (1-\Delta t)\{\tilde{W}_n\} + \Delta t(1-\Delta t)[K]\{v_n\} + \Delta t \int_0^l Z_n[B]^T[B]\{v_n\}\,dx \\
\{v_{n+1}\} - \zeta\Delta t\{a_{n+1}\} = \{v_n\} + (1-\zeta)\Delta t\{a_n\} \ ,
\end{gathered} \tag{27}$$

after each cycle of which, Z_{n+1} is obtained from Eq. (16) ($\tilde{\sigma}_{n+1} = \sigma_{n+1}$); though it is not necessary for algorithmic closure, σ_{n+1} can be obtained from Eq. (19) after each cycle. The frozen coefficient form of Eq. (27) is

$$\begin{gathered}
[M]\{a_{n+1}\} + (\varepsilon + \Delta t)[K]\{v_{n+1}\} + \{\tilde{W}_{n+1}\} = \{\mathbf{0}\} \\
\{\tilde{W}_{n+1}\} = (1-\Delta t)\{\tilde{W}_n\} + \Delta t(1-\Delta t)[K]\{v_n\} + \Delta t Z[K]\{v_n\} \\
\{v_{n+1}\} - \zeta\Delta t\{a_{n+1}\} = \{v_n\} + (1-\zeta)\Delta t\{a_n\} \ .
\end{gathered} \tag{28}$$

Note that for the current scheme σ_n, Z_n and $(v_x)_n = [B]\{v_n\}$ are all piecewise constant in x.

— *Modal decomposition:* Let $[\Psi]$ be a matrix of generalized eigenvectors of $[K] - s[M]$, normalized so that

$$\begin{aligned}
[\Psi]^T[K][\Psi] &= [\Omega] = \mathrm{diag}(\omega_i{}^2) \\
[\Psi]^T[M][\Psi] &= [I] \ .
\end{aligned} \tag{29}$$

We will investigate the stability of the frozen coefficient linearized system. Let

$$\begin{aligned}
\{a_{n+1}\} &= [\Psi]\{\hat{a}_{n+1}\} \\
\{v_{n+1}\} &= [\Psi]\{\hat{v}_{n+1}\} \ .
\end{aligned} \tag{30}$$

The momentum equation gives

$$\{\hat{a}_{n+1}\} + (\varepsilon + \Delta t)[\Omega]\{\hat{v}_{n+1}\} + \{\hat{\tilde{W}}_{n+1}\} = \{0\} \ , \tag{31}$$

where

$$\{\hat{\tilde{W}}_{n+1}\} = [\Psi]^T\{\tilde{W}_{n+1}\} \ . \tag{32}$$

Suppressing the subscript "i" and writing a typical component of $\{\hat{a}_{n+1}\}$ as simply a_{n+1}, etc. The decoupled system is

$$\begin{aligned} &a_{n+1} + (\varepsilon + \Delta t)\omega^2 v_{n+1} + \tilde{W}_{n+1} = 0 \\ &\tilde{W}_{n+1} = (1 - \Delta t)\tilde{W}_n + \Delta t(1 - \Delta t)\omega^2 v_n + \Delta t Z \omega^2 v_n \\ &v_{n+1} - \zeta \Delta t a_{n+1} = v_n + (1 - \zeta)\Delta t a_n \ . \end{aligned} \tag{33}$$

Though $\omega = 0$ is ruled out by boundary conditions in the problems considered here, the lowest frequencies in the mesh are physically meaningful, and the $\omega \to 0$ limit must be considered. It is easy to see with our simple elements [11,12] that the highest frequencies are mesh-dependent, and

$$\omega^2_{\max} \cong \max_i \left(\frac{4}{\alpha L_i{}^2} \right) \ . \tag{34}$$

D. Stability analysis: The goals of stability analysis are twofold: first, to give a prior estimate of the critical time step, if any, and second, to assure that the numerical method does not have the effect of artificially suppressing or delaying the onset of the instability. The onset of spurt corresponds to the instability of the frozen-coefficient linearization. We will then analyze the discrete system (33) applied to the same frozen-coefficient system and find that the instability in the discrete system occurs at precisely the same values of the parameters as the exact linearized system. The exact solution can be expanded in Fourier series; a typical mode is

$$v(x,t) = f(t)\sin\omega x \qquad \sigma(x,t) = g(t)\cos\omega x \ . \tag{35}$$

Substituting into system (2)

$$\begin{aligned} \alpha f'(t) &= -\varepsilon\omega^2 f(t) - g(t)\omega \\ g'(t) &= (Z+1)\omega f(t) - g(t) \ . \end{aligned} \tag{36}$$

The system eigenvalues are

$$s = -\frac{\varepsilon\omega^2/\alpha + 1}{2} \pm \sqrt{\frac{(\varepsilon\omega^2/\alpha + 1)^2}{4} - \frac{(Z + 1 + \varepsilon)\omega^2}{\alpha}} \ . \tag{37}$$

$\mathrm{Re}\, s_{\mathrm{crit}} \leq 0$ only if $Z + 1 + \varepsilon \geq 0$ (decaying solutions) — the Equation Stability Condition. The phase-plane analysis of Refs. [6,7] shows that this condition is the same condition that characterizes the end of the 'latency' period and the onset of the spurt instability. We shall derive stability bounds assuming that $\omega \in (0, +\infty)$.

— *The stress relaxation condition:* The recursion for $\tilde{W}_n$ is based on the underlying O.D.E. for σ, which in time-discrete form is

$$\sigma_{n+1} = (1 - \Delta t)\sigma_n + \Delta t(Z_n(v_x)_n + (v_x)_{n+1}) \ , \tag{38}$$

which, when there is no flow, is

$$\sigma_{n+1} = (1 - \Delta t)\sigma_n \ . \tag{39}$$

This is a discretization of (exponential) stress relaxation, the most fundamental non-Newtonian phenomenon. It is no restriction to assume that Δt is always small enough for accurate stress relaxation. The non-oscillatory stress relaxation condition (NOSRC) is then,

$$\Delta t < 1 \ . \tag{40}$$

The NOSRC is necessary to accurately reproduce the lowest frequency phenomena. To analyze the stability of higher frequencies, we write the first equation of Eqs. (33) in step n and $n+1$; solving this for a_n, a_{n+1} and substituting into the remaining equations of the system (33), results in the following 2x2 system:

$$\begin{Bmatrix} \tilde{W}_{n+1} \\ v_{n+1} \end{Bmatrix} = [\mathbf{A}] \begin{Bmatrix} \tilde{W}_n \\ v_n \end{Bmatrix} \ , \tag{41}$$

where

$$\begin{aligned} [\mathbf{A}] &= \begin{bmatrix} \theta & \Delta t\omega^2(Z+\theta) \\ \frac{\theta\zeta\Delta t + (1-\zeta)\Delta t}{\Delta} & \frac{\zeta\Delta t^2\omega^2(Z+\theta) + \beta - 1}{\Delta} \end{bmatrix} \\ \theta &= \theta(\Delta t) = (1 - \Delta t) \\ \beta &= (1-\zeta)\Delta t\bar{\varepsilon}\omega^2 \\ \Delta &= 1 - \zeta\Delta t\bar{\varepsilon}\omega^2 \\ \bar{\varepsilon} &= \varepsilon + \Delta t \ . \end{aligned} \tag{42}$$

We can bound the spectral radius by using the invariants of $[\mathbf{A}]$ (see [11,12]):

$$\begin{aligned} a_1 &= \frac{1}{2}tr[\mathbf{A}] = \frac{1}{2}\left[\theta + \frac{\zeta\Delta t^2\omega^2(Z+\theta) + \beta - 1}{\Delta}\right] \\ a_2 &= \det[\mathbf{A}] = \frac{1}{\Delta}\left[\theta(\beta - 1) - (1-\zeta)\Delta t^2\omega^2(Z+\theta)\right] \ . \end{aligned} \tag{43}$$

Spectral radius of $[\mathbf{A}]$ being ≤ 1 is characterized by [11,12]

$$-\frac{a_2+1}{2} \leq a_1 \leq \frac{a_2+1}{2}, \ a_2 < 1 \ , \tag{44}$$

and algebraic growth is ruled out by

$$-1 < a_1 < 1, \ a_2 = 1 \ . \tag{45}$$

— *Extreme frequencies:* It turns out that by considering the $\omega \to 0$ and $\omega \to \infty$ behavior of Eqs. (43) - (45), the most salient features of the method described here can be identified; a more detailed analysis is given elsewhere [16]. When $\omega \to 0$ we find that

$$a_1 \to \frac{1}{2}(\theta + 1), \qquad a_2 \to \theta \; .$$

The roots of equation,

$$s^2 - 2a_1 s + a_2 = 0 \; , \tag{46}$$

are θ, and 1; thus requiring $|\theta| \leq 1$ implies $\Delta t \leq 2$. This condition is irrelevant, since the NOSRC supercedes.

When $\omega \to \infty$,

$$\beta \to \pm\infty, \qquad \frac{\beta - 1}{\Delta} \to -\frac{(1-\zeta)}{\zeta} \; ,$$

and

$$\frac{(Z+\theta)\Delta t^2 \omega^2}{\Delta} \to -\frac{(Z+\theta)\Delta t}{\zeta \bar{\varepsilon}} \; ;$$

so

$$a_1 \to \frac{1}{2}\left[\theta - \frac{(Z+\theta)\Delta t}{\bar{\varepsilon}} - \frac{1-\zeta}{\zeta}\right] \; ,$$

$$a_2 \to -\frac{\theta(1-\zeta)}{\zeta} + \frac{(1-\zeta)}{\zeta}\frac{(Z+\theta)\Delta t}{\bar{\varepsilon}} \; .$$

Thus the quadratic Eq. (46) has roots

$$s = \frac{(1-\zeta)}{\zeta}, \quad -\theta + \frac{(Z+\theta)\Delta t}{\bar{\varepsilon}} \; . \tag{47}$$

For $\zeta < 1/2$ conditional stability is anticipated, and specific analysis for large ω is required. This analysis is carried out in detail in Ref. [16], where it is found that there is a dependence of Δt on Δx^2 that is characteristic of parabolic problems [11,12], arising from the Newtonian viscosity term. Since the algorithm is semi-implicit and requires the factorization of matrices, there is no gain in taking $\zeta < 1/2$. In Ref. [16], it is also shown that for $\zeta \geq 1/2$, there are no interior values of the spectral radius between $\omega = 0$ and $\omega = \infty$ higher than those bounded by the NOSRC and by requiring that the roots of Eq. (47) be less than or equal to 1. This implies the following stability summary for $\zeta \geq 1/2$:

(1) From $-\theta + (Z+\theta)\Delta t/\bar{\varepsilon} \leq 1$, we deduce that $(\varepsilon + Z - 1)\Delta t - 2\varepsilon \leq 0$. If $\varepsilon + Z - 1 \leq 0$, there is no condition. Otherwise

$$\Delta t \leq \frac{2\varepsilon}{\varepsilon + Z - 1} \; .$$

(2) From $-\theta + (Z+\theta)\Delta t/\bar{\varepsilon} \geq -1$, we deduce that $(Z+1+\varepsilon)\Delta t \geq 0$. If $Z+1+\varepsilon \geq 0$, there is no condition. Otherwise the numerical method *and* the linearized equations are unstable.

From the phase plane analysis of Refs. [5,6,7], it can be deduced that for the range of parameter space appropriate for modeling Vinogradov's polyisoprenes [13], Z is always negative unless it is forced to be positive by artificial initial conditions. Furthermore, $Z < 0$ whenever the primary normal stress difference, N_1, is positive, as it is for any steady flow of a Johnson-Segalman fluid. Circumstances in which Case (1) above would hold require that N_1 be substantially negative and have not been observed by the authors. However, the linearized equations do not account for the Z-equation, thus could apply equally well to a shear thickening fluid in which $Z > 0$ is likely; in such cases, the condition of Case (1) could apply. In Case (2), whenever the Equation Stability Condition holds, the algorithm is essentially unconditionally stable for all time steps smaller than that implied by the NOSRC, which is an accuracy condition, independent of Δx. When the exact equations are unstable, the numerical method also reproduces solutions that grow rather than decay in time. Thus the onset of the spurt instability is not suppressed by an artificial, numerical increase in the value of $Z+1+\varepsilon$.

The key to the success of the algorithm lies in the first equation of system (27) that predicts the extra stress using the zero shear viscosity implicitly and the non-Newtonian contribution, represented by the nonlinear Z term, explicitly. No nonlinear equations are solved when time is advanced according to the second equation of system (27) , but the fastest wave speed is that at zero shear, as can be seen from Eq. (3) and the fact that $Z \leq 0$. There is no restriction on the time step in the linear stability analysis of Eqs. (6) - (13), and in practice, time steps as large as a half million element wave traversals can be stably employed. However, the analysis of Refs. [5,6,7] shows that when ε is small, the shear-flow problem is extremely stiff; there is a characteristic response time of the system of $O(\varepsilon)$ (the "Newtonian phase") in which the polymer contribution to the shear stress, σ, develops. During this short period, Z changes substantially but then continues to change on a time scale that is typically much longer, determined by the dominant relaxation time, which is scaled to 1 in the nondimensional equations. In order for the slow change in Z to be accurately resolved, the short-time change in Z must have been accurately resolved. In Ref. [5] it is shown that the stiffness requires time steps on the order of fractions of ε at early times to obtain accurate solutions. Time steps can be lengthened somewhat during a quiescent period ("latency"), but, as shown in Refs. [6,7], the $O(\varepsilon)$ scale reemerges in the dynamic spurt process. The point is that the semi-implicitness can be used to accurately smooth out wave propagation at early time, since elastic waves play no important role in the spurt phenomenon; however, this leaves an intricate interplay between two additional, widely separated, time scales that must be properly accounted for in numerical solutions.

3. NUMERICAL RESULTS FOR STEP STRAINS IN SHEAR FLOW

To summarize what occurs in numerical simulations: when $\varepsilon \neq 0$, the total shear stress, T, has a near δ-function contribution, and for $t > 0$ there is spatially homogeneous stress relaxation when $a = 1$. Spatial inhomogeneity develops for $a < 1$ (at sufficiently large γ [10]). With $\varepsilon = 0$, the stresses are bounded for all time if $a = 1$, but there is

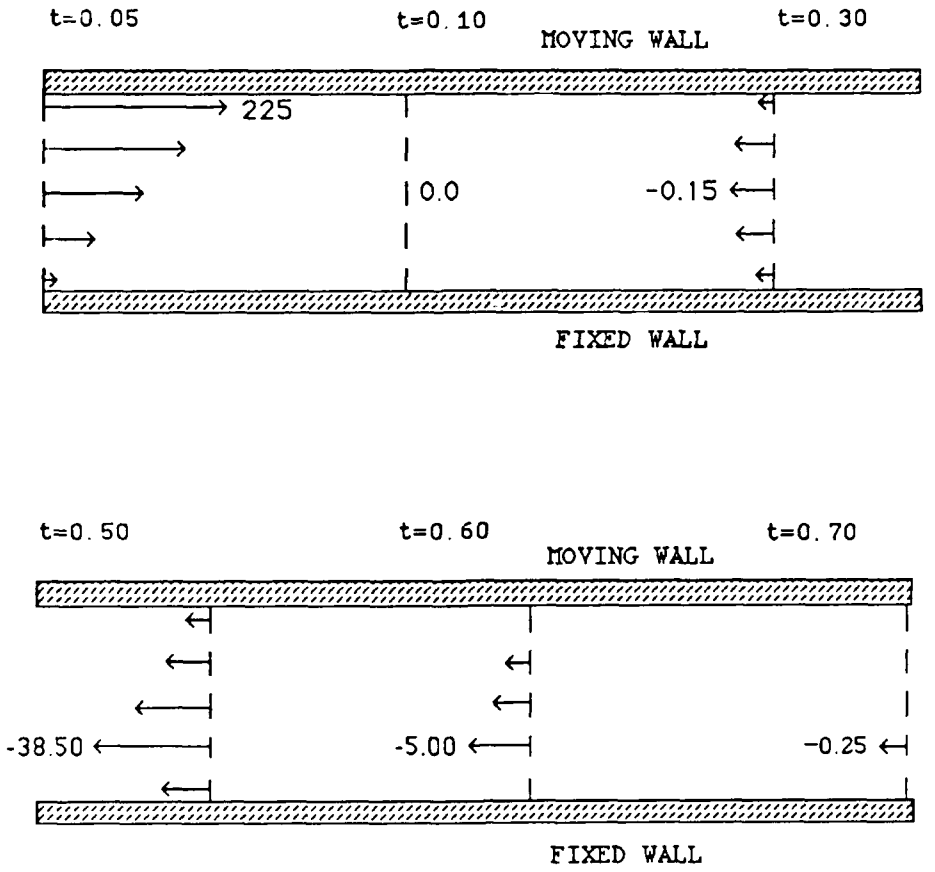

Fig. 5. Velocity profile as time evolves for dynamic solution of system (2) with boundary conditions (4), $a = O(10^{-12})$, $a = 0.95$, $\varepsilon = 0.001417$, and a step of duration 0.1 sec. At this average strain of $\gamma = 12$, the solution develops a spatial inhomogeneity in a latent spurt with flow in the opposite direction from plate motion. The fixed wall is at $x = 0$ and the moving wall at $x = 1$.

Hadamard instability if $a < 1$ and γ is sufficiently large. Thus the effect of Newtonian viscosity is significant. For $a = 1$, its presence does not make a difference in the satisfaction of the Lodge-Meissner relation, but it does make an increasingly large difference in the total force required to move the plate as the steps approach instantaneous rise. For $a < 1$, the Lodge-Meissner relation is not satisfied at large strain, but in the presence of Newtonian viscosity, the computed solutions at large strain are not necessarily unphysical, as has been claimed [15]. As is described in Ref. [10], the failure to satisfy the relation can be associated with an inhomogeneous flow regime that develops some time after plate motion has ceased (Figs. 5 - 7).

Apparently a similar phenomenon to spurt occurs in flows of a Johnson-Segalman fluid after a sudden step in strain. This is illustrated in Fig. 5: There is an initial period in which an essentially homogeneous flow occurs. For smaller strains, roughly $\gamma < 5$ for data corresponding to Vinogradov, et al.'s polyisoprenes, the homogeneity persists for

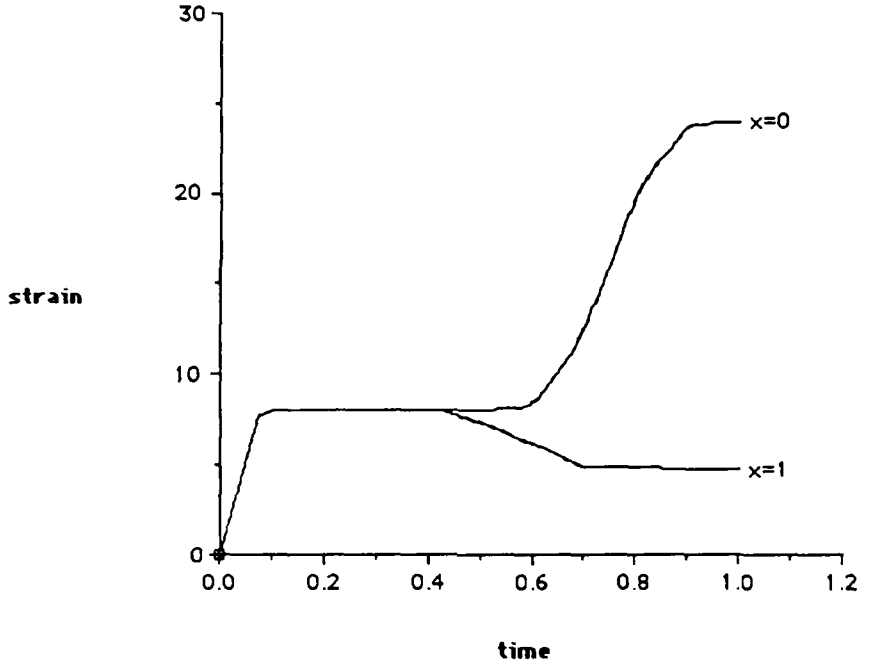

Fig. 6. Local strain at the walls vs. time for dynamic solution of system (2), with boundary conditions (4), $a = O(10^{-12})$, $a = 0.95$, $\varepsilon = 0.001417$, and a step of duration 0.1 sec. At this average strain of $\gamma = 8$, the solution is inhomogeneous at long times.

all time. For moderate strains, roughly $5 < \gamma < 10$ for Vinogradov's data, a spurt-like inhomogeneous flow develops while the stresses are relaxing and the flow has essentially ceased. At moderate strains, the spurt is in the direction of plate motion. For large strains, roughly $\gamma > 10$, the spurt is in the opposite direction from the plate motion, as it is in Fig. 5. These observations explain the inhomogeneity in local strain based on fluid motion of Figs. 6 and 7 (in contrast to γ, an average strain, based on plate motion). It is interesting to note that the formula of Fig. 3 is derived by ignoring momentum effects that are responsible for the development of spatial inhomogeneity, but the position of the pole in that formula correctly predicts the direction of the spurt. These phenomena are not fully understood at the time of this writing, but it seems clear that the criticisms of the Johnson-Segalman model based on assumptions of spatial homogeneity are too simplistic.

4. HIGHER DIMENSIONAL FLOWS - FIBER DRAWING AND 2-D

To generalize these ideas to multidimensional flow requires approximation of the stress gradients in the convected derivative of Eqs. (1). These can be avoided by observing that the effective strain tensor [3(p. 486)] of the Johnson-Segalman model satisfies

$$\begin{cases} \dot{\mathbf{E}}_t(t') = -\mathbf{E}_t(t')\,(a\dot{\mathbf{e}} - \boldsymbol{\omega})\,(t') \\ \mathbf{E}_t(t) = \mathbf{I}\,, \end{cases} \tag{48}$$

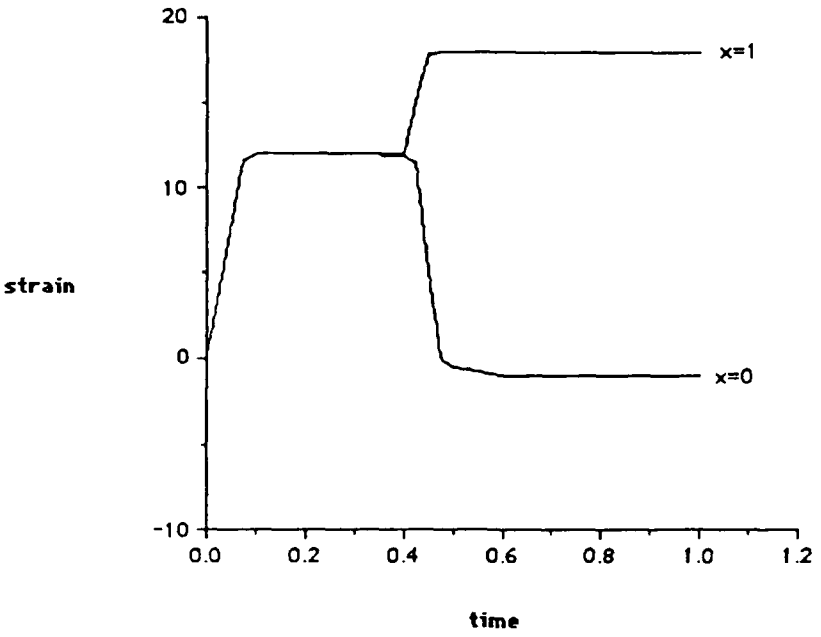

Fig. 7. Local strain at the walls vs. time for dynamic solution of system (2) with boundary conditions (4), $a = O(10^{-12})$, $a = 0.95$, $\varepsilon = 0.001417$, and a step of duration 0.1 sec. At this average strain of $\gamma = 12$, the solution is inhomogeneous at long times, but the inhomogeneity is reversed from what it is for strains on the other side of the pole in the Lodge-Meissner function (see Fig. 3).

where t' represents historical time, and ω is the spin tensor. A Lagrangian difference quotient along particle pathlines can be used to approximate the whole convected derivative of system (1) [3(p. 494)], and the time-discrete stress equations become

$$\frac{\mathcal{D}_a \tau}{\mathcal{D}t} \approx \frac{\tau^{n+1} - E_{t+\Delta t}(t)\hat{\tau}^n E^T_{t+\Delta t}(t)}{\Delta t} = 2\dot{\mathbf{e}}^{n+1} - \tau^n \,, \tag{49}$$

where

$$\hat{\tau}^n := \tau(\mathbf{x}(t), t)\,, \qquad \tau^n := \tau(\mathbf{x}(t+\Delta t), t)\,, \qquad \tau^{n+1} := \tau(\mathbf{x}(t+\Delta t), t+\Delta t))\ . \tag{50}$$

Since this formulation represents an approximation to the Oldroyd derivative [17] as a difference quotient, we refer to it as an "Oldroyd Difference Quotient" (ODQ hereafter). Thus the formulation of the simple shear problem can be employed with piecewise constant stresses, since the full stress gradient field is not required. Existing particle tracking methods can be used to evaluate the required strain tensors [18] with the velocity field held fixed between time steps.

The key to the success of the ODQ formulation of Eqs. (50) is the calculation of an appropriate value of $\hat{\tau}^n$. Eqs. (49) reduce the evaluation of the convected derivative to the one-dimensional calculation of an ordinary derivative along a streamline, but along that streamline, the basic stress approximations are piecewise constant. However, the problem of extracting derivative information from a piecewise constant approximation to a differentiable function of one variable seems preferable to the employment of 2D, C_0 stress fields and the evaluation of (weak) stress gradients. Here we propose scheme based on a transit time-weighted average between the value of the stress in the element containing $\mathbf{x}(t+\Delta t)$ and the value in the adjacent element upwind of $\mathbf{x}(t+\Delta t)$ on the same streamline. The weighting is tuned to recover $O(\Delta t)$ accuracy in Eqs. (49). Approaches to 2D flows that incorporate these features immediately suggest themselves; here we illustrate our approach in the fiber drawing problem of Fig. 9 [19,20]. The mathematical and physical ramifications of this simplified model of fiber drawing have been thoroughly investigated elsewhere (see Refs. [19 – 21], and additional references cited in Ref. [22] for details); furthermore, the finely-tuned methods of Refs. [19] and [20] seem to be the methods of choice for this problem. Our purpose in solving this problem is to illustrate the potential of the ODQ formulation in flows with non-trivial history dependence (i.e., the substantial derivative does not reduce to an ordinary one) in a model problem which can be posed in one spatial dimension, and which results in a relatively small system of PDEs. The problem will also serve to reemphasize the importance of proper numerical treatment of multiple time scales in a rather different context from the shear-flow problem.

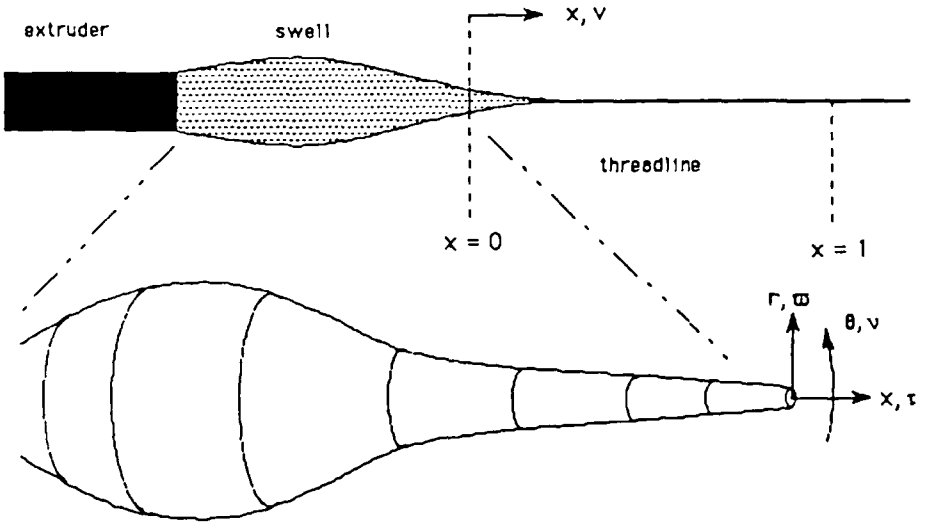

Fig. 8. The domain and coordinate system for the fiber drawing problem.

A. Mathematical formulation: We employ the same nondimensionalization as used for Eqs. (1) and (2); the nondimensional domain is the interval $(0, 1)$, and time is scaled by the relaxation time [2,5], etc. In the problem domain, the polymer contribution to the stress tensor (the extra stress) is assumed to be of the form [21]

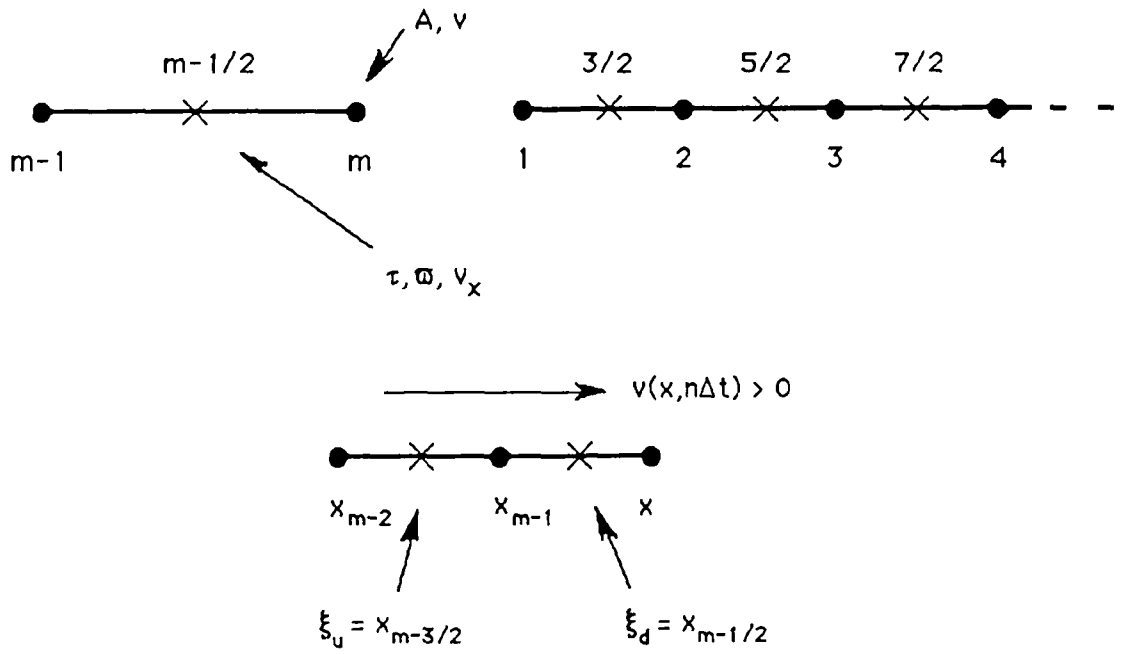

Fig. 9. Staggered grid for fiber drawing problem. Velocity, v and area, A, are at grid points, while stresses, τ and ϖ, and velocity gradient, v_x, are at half-points. Problem makes no sense if velocity changes sign in threadline; positive v assumed.

$$\tau = \begin{bmatrix} \tau & 0 & 0 \\ 0 & \varpi & 0 \\ 0 & 0 & \nu \end{bmatrix} . \tag{51}$$

The velocity field is irrotational with gradients given by

$$\nabla \mathbf{v} = 2\dot{\mathbf{e}} = \begin{bmatrix} v_x & 0 & 0 \\ 0 & -\frac{1}{2}v_x & 0 \\ 0 & 0 & -\frac{1}{2}v_x \end{bmatrix} . \tag{52}$$

The total drawing (x-direction) stress consists of extra stress, pressure (radial stress), and Newtonian contributions:

$$T := N + 3\varepsilon v_x , \tag{53}$$

where

$$N := \tau - \varpi . \tag{54}$$

In terms of these quantities and the area of the fiber, $A(x,t)$, the equations of motion, continuity and stress reduce to a 4x4 system [21], which, combined with boundary conditions is

$$\begin{cases} \alpha A(v_t + vv_x) = (TA)_x \\ A_t + (vA)_x = 0 \\ \tau_t + v\tau_x - 2av_x = -\tau + 2v_x \\ \varpi_t + v\varpi_x + av_x = -\varpi - v_x \\ v(0,t) = D_e, \quad A(0,t) = 1, \quad \tau(0,t) = \tau_0, \quad v_x(0,t) = v_{x0} \ . \end{cases} \tag{55}$$

Our concern here is solution procedures of the stress equations and not the momentum equation, so it is particularly appropriate to eliminate the latter, making the same reduction appropriate to Vinogradov's data [13], which leads to the system of ODEs analyzed in the phase plane in Refs. [5,6,7]. When α is formally set to zero in fiber drawing, however, the result is a 3x3 system of PDEs

$$\begin{cases} A_t = -vA_x - v_x A \\ \tau_t = -v\tau_x - (1 - 2av_x)\tau + 2v_x \\ \varpi_t = -v\varpi_x - (1 + av_x)\varpi - v_x \\ 0 = -v_x + \dfrac{f/A - \tau + \varpi}{3\varepsilon} \ . \end{cases} \tag{56}$$

The fourth equation is an algebraic relation that can be substituted into the first three equations and be integrated with respect to x to give a closed, 3x3, hyperbolic system with integral coefficients. The unknowns are two stresses and the area; the three wave speeds are v.

B. Finite difference discretization: We envisage that future planar and axisymmetric algorithms implementing the ODQ will employ finite element discretization of the momentum equation; in the current reduced problem, it is straight-forward and instructive to use finite differences for all equations of system (55). Motivated by the finite element shear-flow formulation, we use the staggered grid scheme pictured in Fig. 9. This makes stresses and strain rates cell quantities, while area is a grid quantity. The algebraic relation between strain rate and velocity gradient is approximated by

$$\begin{cases} (v_x)^n_{m-\frac{1}{2}} := \dfrac{f/\bar{A}^n - \tau^n_{m-\frac{1}{2}} + \varpi^n_{m-\frac{1}{2}}}{3\varepsilon} \\ \bar{A}^n := \frac{1}{2}\left(A^n_m + A^n_{m-1}\right) \ , \end{cases} \tag{57}$$

while a midpoint rule is used to obtain grid values of velocity.

$$\begin{cases} v^n_1 = D_e \\ v^n_m = v^n_1 + \Delta x \sum_{i=1}^{m-1} (v_x)^n_{i+1/2} \qquad m > 1 \ . \end{cases} \tag{58}$$

An explicit forward in time/backward in space difference scheme is used for the area equation.

$$\begin{cases} \dfrac{A_m^{n+1} - A_m^n}{\Delta t} = -v_m^n \dfrac{A_m^n - A_{m-1}^n}{\Delta x} - (\bar{v}_x)^n A_m^n \\ (\bar{v}_x)^n := \frac{1}{2}\left[(v_x)^n_{m+\frac{1}{2}} + (v_x)^n_{m-\frac{1}{2}} \right] . \end{cases} \tag{59}$$

Turning to the ODQ formulation for the stress equations, we begin by observing that the transit time between two points, x and y, on the threadline in a steady velocity field, $v(x,t) = u(x)$ is given by [23]

$$\delta(x,y) = \int_y^x \frac{d\xi}{u(\xi)} . \tag{60}$$

This is a simple example of a "drift function" [18]; it will be used to define the appropriate components of $\hat{\tau}^n$. Since we intend to apply the ODQ to finite element schemes in the future, it is appropriate to use finite element interpolations of the kind defined using $[N]$ in Sec. 2.C and pictured in Fig. 4 to provide interpolate velocities between grid points. We further approximate velocities as being constant between time steps, so that the steady velocity field $u(x)$ in Eq. (60) will be completely specified by nodal/grid values. Referring to Fig. 9, we find that

$$\delta_1 := \delta(\xi_d, x_{m-1}) = \frac{\ln\left(\frac{1}{2}\left(1 + \frac{v_m}{v_{m-1}}\right)\right)\Delta x}{v_m - v_{m-1}} , \tag{61}$$

and

$$\delta_2 := \delta(x_{m-1}, \xi_u) = \frac{\ln\left(\frac{1}{2}\left(1 + \frac{v_{m-2}}{v_{m-1}}\right)\right)\Delta x}{v_{m-2} - v_{m-1}} . \tag{62}$$

We approximate the logarithms in Eq. (62) by a Taylor series and find that

$$\delta \cong \frac{\frac{1}{2}\left(\frac{v_j}{v_i} - 1\right)\Delta x}{v_j - v_i} = \frac{\Delta x}{2v_i} , \tag{63}$$

where i and j are m, $m-1$, or $m-2$ as indicated by Eq. (62). Note that $\delta_1 = \delta_2 = \Delta x/2v_{m-1}$ the transit time from ξ_u to ξ_d is approximated by $\delta_c := \delta_1 + \delta_2 \cong \Delta x/v_{m-1}$; this will be used to define the appropriate components of $\hat{\tau}^n$.

We now turn our attention to approximation of the strain. Let

$$\kappa := \int_t^{t+\Delta t} v_x\left(x(t'), t'\right) dt' . \tag{64}$$

We use a first-order approximation to the integral:

$$\kappa \cong \begin{cases} \Delta t v_x(\xi_d, t) & \delta_1 > \Delta t \\ \delta_1 v_x(\xi_d, t) + (\Delta t - \delta_1) v_x(\xi_u, t) & \delta_1 \le \Delta t . \end{cases} \tag{65}$$

The two cases represent the situation in which the particle at the centroid of a given element stays in the same element during one time step and the case in which it passes into the next element upstream, respectively.

Note that $\kappa = O(\Delta t)$ during a single time step, and thus a Taylor series expansion for the strains of Eq. (48) is appropriate. The appropriate strains and their Taylor series approximations are then

$$E^2 := \begin{cases} E_{11}^2 = \exp(2a\kappa) \cong 1 + 2a\kappa & s = \tau \\ E_{22}^2 = \exp(-a\kappa) \cong 1 - a\kappa & s = \varpi \ . \end{cases} \tag{66}$$

The following definitions will allow us to specify the ODQ algorithm for a generic stress equation:

$$r := \frac{v_{m-1}^n \Delta t}{\Delta x} \qquad c := \begin{cases} 2 & s = \tau \\ -1 & s = \varpi \end{cases} \qquad b := ca\frac{\kappa}{\Delta t} \ . \tag{67}$$

Note that $|b| = O(1)$ with respect to Δt, and $b = 0$ in the corotational [3], or $a = 0$ case. In terms of b, a generic strain, E is

$$E^2 = 1 + b\Delta t \ . \tag{68}$$

We define a generic stress (either τ or ϖ), $s_{m-1/2}^n$, at time-level n and staggered grid point $m - 1/2$. The appropriate generic component of $\hat{\tau}^n$, $\hat{s}^n$, is defined using r, which can be seen to be the fraction of the transit time from one element centroid to the next that is covered in one time step. Stability restrictions discussed in the next section essentially assure that $r < 1$. $\hat{s}^n$ is defined by

$$\hat{s}^n := (1 - r)s_{m-1/2}^n + rs_{m-3/2}^n \ . \tag{69}$$

We use Eq. (69) and take the two stress equations in the form of Eq. (55); the ODQ method for a generic stress equation is

$$\frac{s_{m-\frac{1}{2}}^{n+1} - (1 + b\Delta t)\left[(1-r)s_{m-\frac{1}{2}}^n + rs_{m-\frac{3}{2}}^n\right]}{\Delta t} = -s_{m-\frac{1}{2}}^n + c(v_x)_{m-\frac{1}{2}}^n \ . \tag{70}$$

Note that the whole left side of the stress equations in Eq. (55) is approximated by the ODQ. For the purposes of analysis, we rearrange Eq. (70) as follows:

$$\begin{aligned} \frac{s_{m-\frac{1}{2}}^{n+1} - s_{m-\frac{1}{2}}^n}{\Delta t} &= -v_{m-1}^n \frac{s_{m-\frac{1}{2}}^n - s_{m-\frac{3}{2}}^n}{\Delta x} \\ &\underbrace{-v_{m-1}^n b\Delta t \frac{s_{m-\frac{1}{2}}^n - s_{m-\frac{3}{2}}^n}{\Delta x}}_{\textit{added term}} - (1-b)s_{m-\frac{1}{2}}^n + c(v_x)_{m-\frac{1}{2}}^n \ . \end{aligned} \tag{71}$$

The ODQ method in this simple problem, with the approximations we have made for transit times and strains is a modified backward difference scheme along the streamline. It reduces to a simple backward difference scheme in the corotational case.

C. Stability analysis: For the purposes of stability analysis, we first study the corotational case where $a = 0$. It is not clear whether this case is physically relevant to actual polymer systems, but the equations are more tractable, and the results of the analysis of this case admit to a straight-forward modification for $a \neq 0$ that works well in practice. In the $a = 0$ case, the discretization of the area equation and ODQ treatment of the stress equations reduces to a backward difference method for the whole system. Since the wave speeds are all v, inspection of Eqs. (56) suggests that a stability bound of $\Delta t \leq \Delta x/v$ is sufficient. This is because, as will be illustrated in the subsequent analysis, the principal part of the system usually dominates the stability bound, while the source terms contribute the effect of an change of $O(\Delta x)$ in v in the conventional bound. Since the conventional bound is slightly pessimistic, a stable and accurate time step can usually be obtained by using a modest safety factor. This is not the case here when ε is small. First, consider the linearized area equation,

$$\delta A_t = -v\delta A_x + \frac{\delta A}{3\varepsilon}N + \frac{A_x}{3\varepsilon}\int_0^x \left(\frac{f\delta A}{A^2} + \delta N\right) dx' + \frac{A}{3\varepsilon}\delta N \ , \tag{72}$$

where the varied quantities are preceded by "δ," and the expansion point by corresponding quantities without δs. The four terms on the right-hand side have the following description: principal part (highest order term), intermediate order source term, low-order (integral) source term, and coupling term (intermediate order), respectively. First we consider the behavior of the linearized area equation uncoupled from the stress equations by taking $\delta N = 0$. A standard Neumann analysis [24,25] shows that the backward difference method applied to the linearized area equation is stable in the sense required for convergence [25(p. 42)] if the conventional bound on Δt is enforced. This restriction, however, allows unbounded growth for $t \to \infty$ on a fixed grid, due to growth of low frequency disturbances. This arises from the fact that the intermediate order term (with coefficient proportional to N) is typically positive. Numerical experiments with the backward difference method applied to Eq. (72) show that the integral term is not sufficient to eliminate the growth of low frequency disturbances. Such unbounded growth *can* be ruled out by the coupling terms, if the linearized stress equations governing δN are stably integrated. We turn our attention to a criterion, based on the stress equations alone, that will prevent blow up of discrete solutions as $t \to \infty$. We pursue this course since we are interested in finding steady solutions on fixed grids.

A simple bound can be derived by further uncoupling the stress equations fr m each other. This bound turns out not to be sufficient, but it illustrates the essence of the problem. We linearize a typical stress equation and set the perturbed quantities from other equations to zero, and, as in the case of the area equation, we ignore the variation of the velocity that is reflected in the lowest order (integral) term. Letting $q := \frac{\Delta t}{\Delta x}$ and considering a disturbance of wave number ω/π in a standard Neumann analysis, yields a growth function, ρ, given by

$$\rho = 1 - qv + qv\exp(-i\omega\Delta x) - \Delta t\left(1 + \frac{|c|}{3\varepsilon}\right) , \tag{73}$$

where v is the velocity field of the expansion point of the linearization. We note that $|\rho|$ is bounded by 1 for $\omega = 0$ if $\Delta t \leq 2/\left(1 + \frac{|c|}{3\varepsilon}\right)$; this restriction is always superseded by the bound arising from $\omega\Delta x = \pm\pi$ (wave number $1/\Delta x$), which turns out to be the most unstable mode. This is

$$\Delta t \leq \frac{\Delta x}{v + \left(1 + \frac{|c|}{3\varepsilon}\right)\frac{\Delta x}{2}} . \tag{74}$$

The bound is most stringent where v is maximum, usually at $x = 1$.

There seems to be no accuracy requirement to make $\Delta x \ll \varepsilon$; good results will be exhibited below in cases where quite the opposite is true. Yet in such cases, the bound of Eq. (74) is much smaller than the conventional bound, and this cannot be avoided in this explicit formulation. What we see is another manifestation of the extreme stiffness induced by a small amount of Newtonian viscosity; in the semi-implicit shear-flow algorithm, it only affects accuracy during those periods of dynamic response when the "Newtonian" time scale is active. In the explicit fiber-drawing algorithm, it affects stability, and the Newtonian time scale must be respected at all times. Since this stiffness arises from the competition of the wave speeds of the principal part with the time scale inherent in the source terms, we have dubbed it "source term stiffness."

Numerical experiments show that the bound of Eq. (74) is over-optimistic by roughly a factor of 3/2. We write the coupled stress equations in matrix form,

$$\left\{U^{n+1}_{m-1/2}\right\} = \left\{U^{n}_{m-1/2}\right\} - vq\left(\left\{U^{n}_{m-1/2}\right\} - \left\{U^{n}_{m-3/2}\right\}\right) - \frac{\Delta t}{3\varepsilon}[\mathcal{B}]\left\{U^{n}_{m-1/2}\right\} , \tag{75}$$

where

$$[\mathcal{B}] = -3\varepsilon\,[I] + \begin{bmatrix} -2 & 2 \\ 1 & -1 \end{bmatrix} . \tag{76}$$

The discrete system (75) is diagonalizable, and the result is an uncoupled system: standard Neumann analysis can be carried out, giving a bound analogous to Eq. (74), in which the $1 + \frac{|c|}{3\varepsilon}$ in the denominator of Eq. (74) is replaced by the magnitude of the most negative eigenvalue of $\frac{1}{3\varepsilon}[\mathcal{B}]$. The result is

$$\Delta t \leq \frac{\Delta x}{v + \left(1 + \frac{1}{\varepsilon}\right)\frac{\Delta x}{2}} . \tag{77}$$

We note that this is the same bound that would result subtracting the two stress equations to produce a single equation for N. The second eigenvalue of $[\mathcal{B}]$ is $O(1)$ (with respect to ε) and is irrelevant to stability. The same trick of combining the equations would not work in the case $a \neq 0$, so that the matrix analysis is necessary. We linearize Eq. (71); as can be seen from the bound of Eq. (77), and as will be evident in the numerical

results presented below, the crucial terms for stability analysis are those of order $O(\varepsilon^{-1})$. The only terms in the discrete equations (71) with $a \neq 0$ that differ from our previous analysis that we chose to include are those of order $O(\varepsilon^{-1})$. These include the terms of order $O(\varepsilon^{-1})$ already accounted for in the analysis of the corotational case and additional terms arising from "δb." Furthermore, among those terms, those that arise from linearizing the "added term" in Eq. (71) are $O(\Delta t)$ smaller than those obtained from linearizing the source term $(1-b)s^n_{m-1/2}$, so we ignore the former and include only the latter. We note that this admittedly *ad-hoc* procedure is equivalent to retaining only $O(\varepsilon^{-1})$ terms in the linearization of Eqs. (56) and applying a backward difference scheme (without the "added term") to the result; this has the effect of replacing $[\mathcal{B}]$ by

$$[\mathcal{B}] = -3\varepsilon\,[I] + \begin{bmatrix} -2(1+a\tau) & 2(1+a\tau) \\ (1+a\varpi) & -(1+a\varpi) \end{bmatrix} \tag{78}$$

resulting in the modified bound,

$$\Delta t \leq \frac{\Delta x}{v + \left(1 + \frac{1+a\left(\tau - \frac{N}{3}\right)}{\varepsilon}\right)\frac{\Delta x}{2}} \,. \tag{79}$$

The reason we opt for this *ad-hoc* bound is that it provides a simple modification of the bound of Eq. (77) and avoids the solution of a quadratic equation at each time step, which would be necessitated by a consistent analysis. As demonstrated in the next subsection, this bound is very good for $a = 0$ and only slightly pessimistic for $a \neq 0$. We should also point out that, from Eqs. (65) and (71) and from the fact that the added term in Eq. (71) is $O(\Delta t)$, it is an easy matter to verify that the ODQ method is consistent but no more than first order accurate.

D. Numerical results: Figs. 10 — 13 summarize the stability and accuracy of the ODQ method for fiber drawing. For a discussion of the nature of the results and their physical interpretation, see Ref. [22]. The results displayed in these figures were obtained by using the bound of Eq. (79) to compute a virtually steady solution, which was saved for the stability and accuracy studies. The "true" stable time step, labelled Δt on the plots, was obtained by interval halving from a bracket obtained by incrementing the bound of Eq. (79) by a sufficient amount to obtain an unstable step. The Δt reported is the last stable time step observed at the point where the bracket had been reduced to a small enough size to make no difference to graphical accuracy. The stable time step thus calculated applies only to the specific steady solution involved, but the bound of Eq. (79) has been found to be sufficient for stability throughout dynamic processes leading to steady solutions. The convergence plots were obtained from an estimate of the exact solution obtained by Richardson extrapolation to $O(\Delta x^3)$. Since the expected accuracy is first order, and the extrapolations to second order agree very closely with the extrapolations to third order, the assumption that the values extrapolated to third order are exact with respect to the raw, first order results seems well-justified. Note that the plotted errors are absolute errors, and the relative errors are quite acceptable with 100 grid cells.

There are two major points to be made, based on the numerical results: First, the stability bound of Eq. (79) works well, and second, with small ε, acceptably accurate

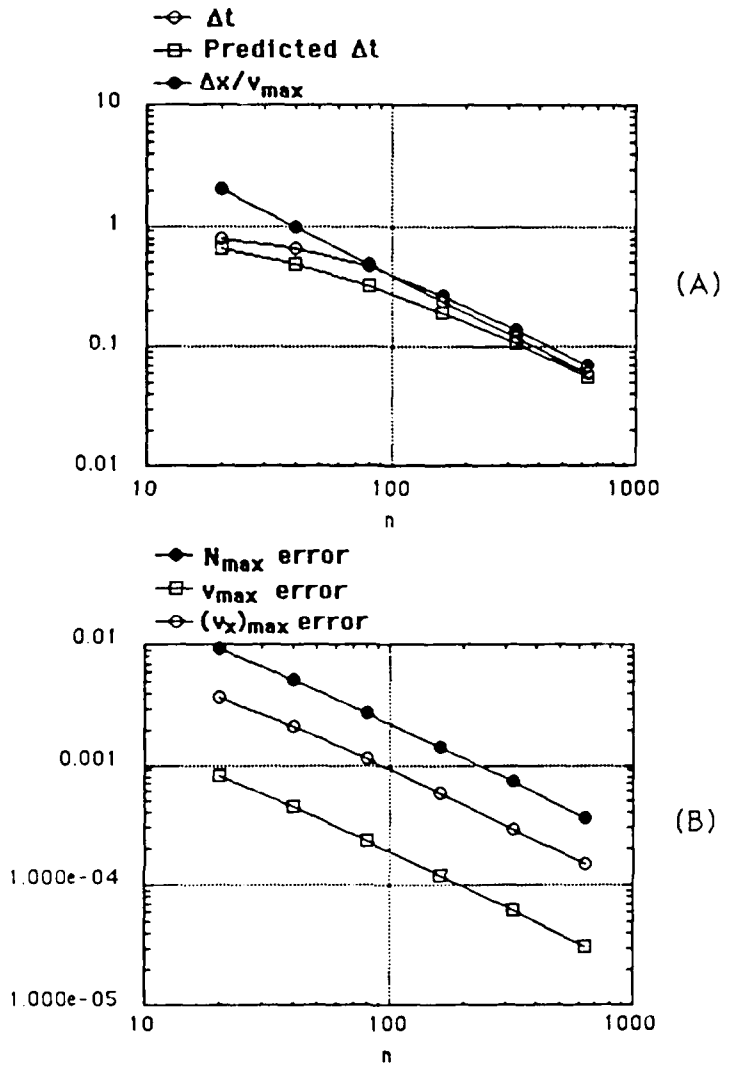

Fig. 10. Mesh Refinement Studies — Corotational ($a = 0$) Case: (A) Actual Δt, compared Δt predicted by the stability bound of Eq. (79), and to the usual wave-speed bound, in the for the $\varepsilon = 1$ case. (B) Convergence rate of maximum values of key quantities to the value obtained by multi-mesh extrapolation. Slope is essentially -1, indicating a first-order method.

results are obtained long before the conventional bound of $\Delta t \leq \Delta x/v$ becomes useful on very fine meshes; thus, the bound of Eq. (79) is necessary to obtain solutions in the practical operating range of the method. Fig. 10 shows the corotational case with a large ε; there is no stiffness in this case, and as indicated in panel (A), the conventional bound becomes adequate on meshes of 80 grid points or more and could be used generally with a modest safety factor. The expected first order convergence rate with grid refinement is confirmed here and in all other cases. The stability situation is markedly different with small ε, as illustrated in Fig. (11). With 80 to 100 grid points, where solution accuracy is quite good, the stability bound of Eq. (79) is very sharp and differs substantially from

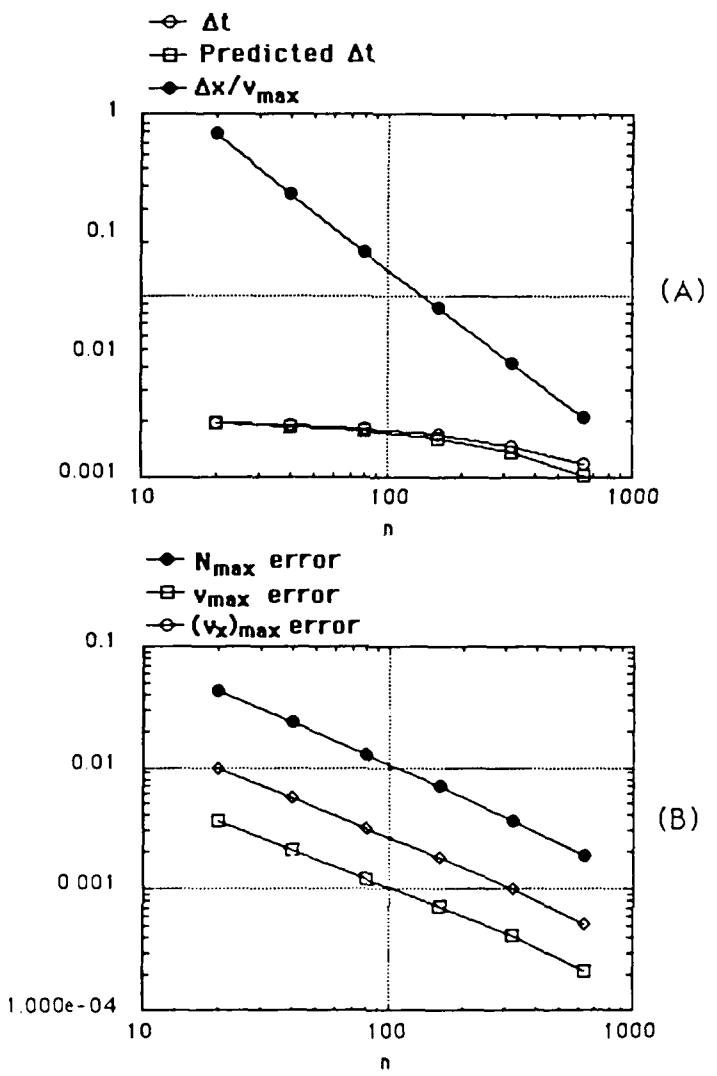

Fig. 11. Mesh Refinement Studies — Corotational ($a = 0$) Case: (A) Actual Δt, compared Δt predicted by the stability bound of Eq. (79), and to the usual wave-speed bound, in the for the $\varepsilon = 0.01$ case. (B) Convergence rate of maximum values of key quantities to the value obtained by multi-mesh extrapolation. Slope is essentially -1, indicating a first-order method.

the conventional bound; steady solutions could not be obtained on such grids using the conventional bound.

In the upper convected case with large ε shown in Fig. (12), the conventional bound is conservative, and the bound of Eq. (79) is slightly more so, but both bounds do well. When ε is small (Fig. (13)), the conventional bound is over optimistic until the grid has 640 points. The bound of Eq. (79) is slightly conservative, but does well throughout this range. For grids finer than 640 points, it appears that, as with the large ε case, the conventional bound is becoming a viable bound, slightly less pessimistic than the bound of Eq. (79); however for very fine grids, both bounds are essentially the same. From a

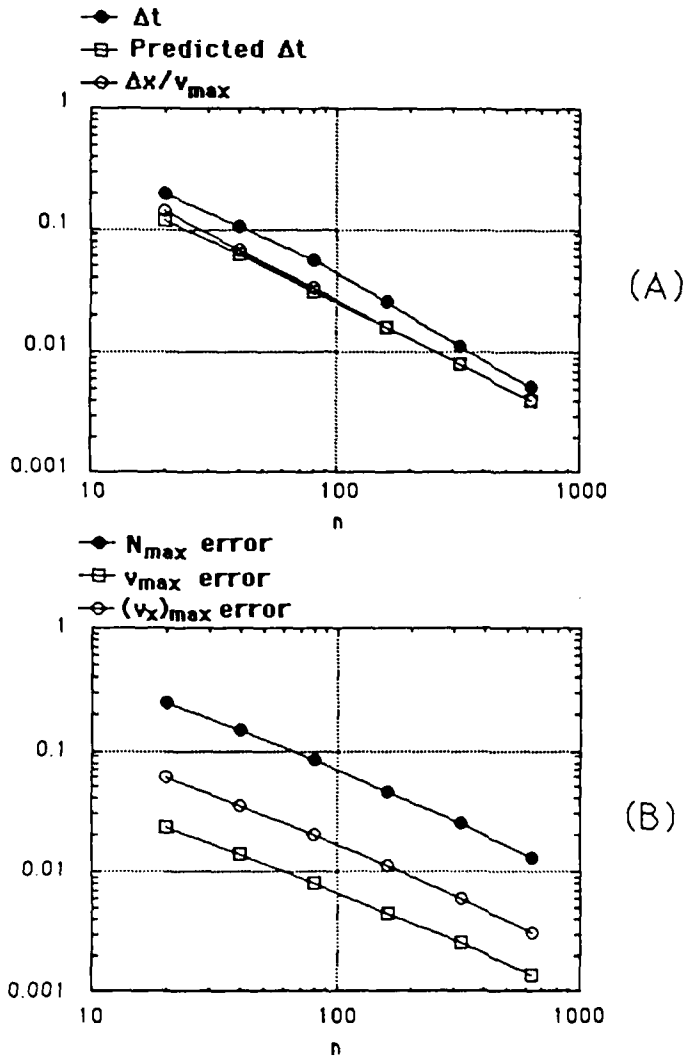

Fig. 12. Mesh Refinement Studies — Upper Convected ($a = 1$) Case: (A) Actual Δt, compared Δt predicted by the stability bound of Eq. (79), and to the usual wave-speed bound, in the for the $\varepsilon = 1$ case. (B) Convergence rate of maximum values of key quantities to the value obtained by multi-mesh extrapolation. Slope is essentially -1, indicating a first-order method.

practical standpoint, the bound of Eq. (79) is sufficient throughout the range of realistic grids and is always relatively sharp.

5. CONCLUSIONS

Much of what we know about the spurt phenomenon in Poiseuille flow is now accessible to analysis but was first uncovered by numerical simulation. We hope that a similar situation will come about in the analysis of step-strain experiments. Our preliminary numerical investigation suggests that a deeper analysis using non-monotone constitutive equations would be worthwhile. From a rheological point of view, it is important to discover whether the failure to satisfy the Lodge-Meissner relation is an indication of

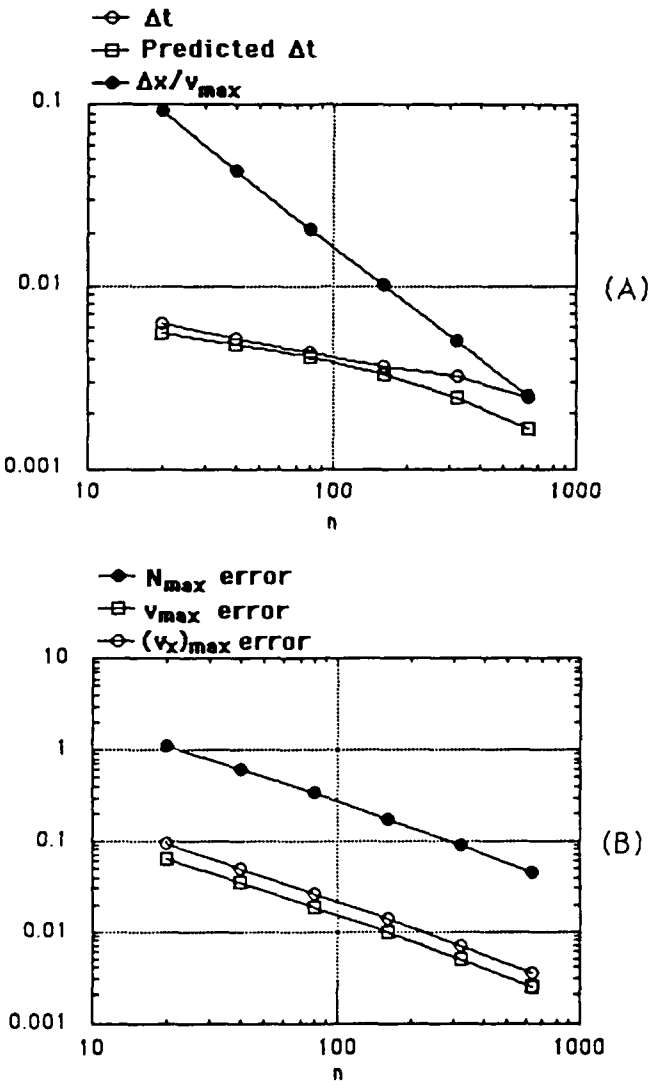

Fig. 13. Mesh Refinement Studies — Upper Convected ($a = 1$) Case: (A) Actual Δt, compared Δt predicted by the stability bound of Eq. (79), and to the usual wave-speed bound, in the for the $\varepsilon = 0.01$ case. (B) Convergence rate of maximum values of key quantities to the value obtained by multi-mesh extrapolation. Slope is essentially -1, indicating a first-order method.

defect in the constitutive equation, as is widely believed, or the failure represents a success of the constitutive equation in predicting a new kind of material response to step strains that can occur in certain (perhaps extreme) conditions. Our numerical simulations have made the connection between material response in step strain and the spurt phenomenon that may prove important in resolving this rheological controversy.

From a technical point of view, the major conclusion is that the Newtonian time scale must always be respected. When this is very short compared to the dominant relaxation time, the resulting stiffness affects accuracy alone for the implicit-explicit shear flow

method. This stiffness affects stability and accuracy for the ODQ method. In either case, $\Delta t = O(\varepsilon)$ is often called for. Fortunately, however, in the problems we have solved so far, mesh size scales of $O(\varepsilon)$ have not been found necessary; in fact, the major technical problem with source term stiffness is that quite accurate solutions can be obtained on grids that are not fine enough to render the conventional bound on Δt useful.

The ODQ method seems to show some promise. The results we have obtained so far lead us to believe that further study of the ODQ method is warranted.

Acknowledgment: The authors are grateful to M. W. Johnson, B. J. Plohr, and J. A. Nohel for many helpful conversations. They are also grateful to J. C. Strikwerda for a helpful suggestion relating to stability analysis for fiber drawing.

References

1. M. Johnson and D. Segalman, "A Model for Viscoelastic Fluid Behavior which Allows Non-Affine Deformation," *J. Non-Newtonian Fluid Mech.* **2** (1977), pp. 255–270.

2. R. Kolkka, D. Malkus, M. Hansen, G. Ierley, and R. Worthing, "Spurt Phenomena of the Johnson-Segalman Fluid and Related Models," *J. Non-Newtonian Fluid Mech.*, 1988, pp. 303-325.

3. R. Bird, R. Armstrong, O. Hassager, and C. Curtiss, *Dynamics of Polymeric Liquids*, John Wiley and Sons, New York, 1987.

4. R. Kolkka and G. Ierley, "Phase Space Analysis of the Spurt Phenomenon for the Giesekus Viscoelastic Fluid Model," *J. Non-Newtonian Fluid Mech.*, 1989. To appear.

5. D. Malkus, J. Nohel, and B. Plohr, "Dynamics of Shear Flow of a Non-Newtonian Fluid," *J. Comp. Phys.*, 1989. To appear, also CMS Technical Summary Report #89-14.

6. D. Malkus, J. Nohel, and B. Plohr, "Analysis of New Phenomena in Shear Flow of Non-Newtonian Fluids," *Siam. J. Appl. Math.*, 1989. Submitted, also CMS Technical Summary Report #90-6.

7. D. Malkus J. A. Nohel, and B. Plohr, "Quadratic Dynamical Systems Describing Phenomena in Shear Flow of Non-Newtonian Fluids," in *Proceedings IMA Workshop on Nonlinear Evolution Equations That Change Type (Minneapolis, 1989)*, 1989. Submitted, also CMS Technical Summary Report #90-7.

8. D. Joseph, M. Renardy, and J.-C. Saut, "Hyperbolicity and Change of Type in the Flow of Viscoelastic Fluids," *Arch. Rat. Mech. Anal.* **87** (1985), pp. 213–251.

9. W. Hrusa, J. Nohel, and M. Renardy, "Initial Value Problems in Viscoelasticity," *Appl. Mech. Rev.* **41** (1988), pp. 371–378.

10. M. Johnson and D. Malkus, "Shear-Flow Instabilities and Numerical Algorithms for Non-Newtonian Flows," *Math. Mod. Num. Anal.*, 1989. in preparation.

11. R. Cook, D. Malkus, and M. Plesha, *Concepts and Applications of Finite Element Analysis*, John Wiley and Sons, New York, 1989.

12. T. Hughes, *The Finite Element Method*, Prentice-Hall, Englewood Cliffs, 1987.

13. G. Vinogradov, A. Malkin, Yu. Yanovskii, E. Borisenkova, B. Yarlykov, and G. Berezhnaya, "Viscoelastic Properties and Flow of Narrow Distribution Polybutadienes and Polyisoprenes," *J. Polymer Sci., Part A-2* **10** (1972), pp. 1061–1084.

14. A. Lodge, "A Classification of Constitutive Equations Based on Stress Relaxation Predictions for the Single-Jump Shear Strain Experiment," *J. Non-Newt. Fluid Mech.* **14** (1984), pp. 67–83.

15. S. Kahn and R. Larson, "Comparison of Simple Constitutive Equations for Polymer Melts in Shear and Biaxial and Uniaxial Extensions," *J. Rheol.* **31** (1987), pp. 207–234.

16. D. Malkus, and Y.-C. Tsai, "Stability Analysis of Implicit-Explicit Time Integration for Viscoelastic Flow," in preparation, 1989.

17. J. Oldroyd, "Non-Newtonian Effects in Steady Motion of Some Idealized Elastico-Viscous Liquids," *Proc. Roy. Soc. London* **A 245** (1958), pp. 278–297.

18. B. Bernstein, D. Malkus, and E. Olsen, "A Finite Element for Incompressible Plane Flows of Fluids with Memory," *Int. J. Num. Meth. Fluids* **5** (1985), pp. 43–70.

19. A. Beris and B. Liu, "Time-Dependent Fiber Spinning Equations. 1. Analysis of the Mathematical Behavior," *J. Non-Newt. Fluid Mech.* **26** (1988), pp. 341–361.

20. B. Liu and A. Beris, "Time-Dependent Fiber Spinning Equations. 2. Analysis of the Stability of Numerical Approximations," *J. Non-Newt. Fluid. Mech.* **26** (1988), pp. 363–394.

21. C. Petrie, *Elongational Flows*, Pitman, London, 1979.

22. R. Kolkka, and D. Malkus, "Asymptotic Behavior of a Johnson-Segalman in Steady and Transient Spinning Flow," F.R.O.G. Technical Report #89-32, 1989. To appear.

23. D. Malkus, "Functional Derivatives and Finite Elements for the Steady Spinning of a Non-Newtonian Filament," *J. Non-Newt. Fluid Mech.* **8** (1981), pp. 223–237.

24. R. Richtmeyer, K. Morton, *Difference Methods for Initial-Value Problems*, John Wiley and Sons, New York, 1967.

25. J. Strikwerda, *Finite Difference Schemes and Partial Differential Equations*, Wadsworth and Brooks/Cole, Pacific Grove, 1989.